Experiments in Fluids 13, 249–256 (1992)

Experiments in Fluids

Study of laminar thermal boundary layers occurring around the leading edge of a vertical isothermal wall using a specklegram technique

D. Kastell, K. D. Kihm, and **L. S. Fletcher**

Department of Mechanical Engineering, Texas A & M University, College Station, TX 77843-3123, USA

Abstract. The influence of a 45 degree leading edge on the development of a thermal boundary layer on a vertical isothermal wall has been investigated by measuring detailed temperature profiles with a He–Ne laser specklegram technique. A digital image processor was employed to improve the accuracy in evaluating the space of fringes, which were constructed from the specklegram. A matrix of five different temperatures and four different vertical locations was considered in the investigation. The leading edge effect was evident in the vicinity of the edge ($x = 7.8$ mm and 14.2 mm) showing a strong nonsimilarity, and the thermal boundary layers occurred around the leading edge. Classical theory did not properly describe the actual situation near the leading edge, where the theory assumed an abrupt starting of the boundary layer. In an attempt to improve the agreement in temperature profiles, the Grashof number was modified by extending x to an equivalent plate length x_0. In the region farther from the leading edge ($x = 50.0$ mm), where similarity in temperature profiles was well established, agreement with theory was dramatically improved with substitution of x_0 for x. A linear decrease in the extension ratio x_0/x with $Gr_x^{1/4}$, i.e., $x_0/x = -0.4 \cdot Gr_x^{1/4} + 12.63$ where the Grashof number was based on x, was observed for Grashof numbers up to 8.0×10^5. For $Gr_x \geq 8.0 \times 10^5$, the leading edge effect became negligibly small and the ratio x_0/x approached unity.

List of symbols

a	distance between the test section and the second parabolic mirror (mm)
b	distance between the second mirror and the ground glass (mm)
c	distance between the ground glass and the focal plane of a camera used for specklegram recording (mm)
d	distance between the specklegram negative and the detector plane of a video camera used for the fringe spacing evaluation (mm)
g	acceleration of gravity (9.8 m/s^2)
Gr_x	Grashof number based on $x \left(\equiv \dfrac{g \cdot \beta \cdot (T_w - T_\infty)}{\nu^2} \cdot x^3 \right)$
Gr_{x_0}	Grashof number based on x_0
H	plate height (254 mm)
K	Gladstone-Dale constant for air (0.2257×10^{-3} m^3/kg)
L	plate width measured along the optical axis (254 mm)
m	magnification of the second (parabolic) mirror (b/a)
m'	magnification of the conventional camera lens
n	index of refraction of air
s	fringe spacing measured at the image plane of the video camera (mm)
T	temperature (K)
x	coordinate parallel to the vertical plate (mm)
x_0	equivalent plate-length used to improve the comparison of data with theory (mm)
y	coordinate perpendicular to the vertical plate (mm)
z	coordinate parallel to the optical axis (mm)
α	refraction angle of a light ray after passing the test section
β	coefficient of thermal volumetric expansion (K^{-1})
ε	incident angle of the refracted ray toward the ground glass
δ	fringe spacing at the focal plane of the camera or the thermal boundary layer thickness (mm)
θ	dimensionless temperature function $\left(\theta = \dfrac{T - T_\infty}{T_w - T_\infty} \right)$
η	dimensionless similarity variable $\eta = \dfrac{y}{x} \cdot \left(\dfrac{Gr_x}{4} \right)^{1/4}$
ϱ	air density (kg/m^3)
λ	wavelength of He = Ne laser (632.8 nm)
Δ	speckle translocation on the specklegram
ν	kinematic viscosity of air (m^2/s)

1 Introduction

For most heat convection problems, once precise data on temperature profiles in the thermal layers are acquired, correlations between the heat transfer coefficients can readily be determined with limited additional effort. The conventional method involves the use of the total heat flux to determine the correlation coefficients. When the heaters are well insulated to provide an isoflux condition, the method provides fairly good accuracy. For the case of an isothermal surface, it is very difficult and cumbersome to attain a precise heat flux measurement since the temperature gradient at the surface must be measured without disturbing the thermal layer. The introduction of thermocouple probes into the thermal layer on an isothermal wall will result in significant flow and thermal disturbances.

Various interferometry techniques (Vest, 1979) have been used for an in-situ measurement of temperature profiles in thermal layers. In the present study, a more advanced and accurate optical tool, a specklegram or speckle photography technique (Dainty, 1984) has been employed for the measurement. The specklegram technique, which shares the fundamental optical principle of light refraction in a nonuniform density medium, has several advantages over interferometry.

The specklegram system, in general, is relatively simple to construct and more straightforward to align. The most important asset of speckle photography is in its excellent resolution of temperature data. The resolution of temperature measurements by interferometry is limited by the number of fringes on the interferogram, which is finite and pre-specified from the optical configuration. The resolution of specklegram data points, however, is far superior because the specklegram is scanned with a laser beam of small cross-sectional area to generate an instantaneous fringe pattern at each data point (Wernekinck and Merzkirch, 1986). Also, the quantification process of a specklegram is simpler than that of an interferogram. Interferograms are analyzed by a densitometer to measure the spacing and the direction of fringes. This procedure is very tedious and also has a high probability of causing nontrivial inaccuracy. The evaluation of the fringe spacing for specklegrams can be done by a digital image analyzer system for better accuracy and faster processing (Erbeck, 1985).

In measuring temperature profiles, non-ideal factors of experimental configurations such as the non-zero thermal boundary layer thickness at a leading edge, must be carefully considered and minimized for correct comparison of the data with theory. Since Pohlhausen (1921) initiated the heat transfer study of a vertical plate, most theoretical studies have assumed an ideal leading edge with zero thickness of the thermal boundary layer (Ostrach, 1952, and others). Using a Mach-Zehnder interferometer, Eckert and Soehngen (1948) showed qualitatively that the thermal boundary layer extended all around the lower end of the vertical heated plate. Scherberg (1962) showed that the temperature distribution in the thermal boundary layer along a vertical isothermal plate can be significantly different depending upon the leading edge geometry. A series of studies by Yang and Jerger (1964), Suriano et al. (1965), and Suriano and Yang (1968) studied the problem using perturbation techniques or finite difference methods, and they showed a departure of their solutions from the ideal solution when the Grashof number was less than about 10^3. The fact that free convection starts before the origin of an isothermal vertical wall was clearly evident in a Wollaston prism interferometric visualization study conducted by Sernas et al. (1972). Grizagoridis (1973, 1978) experimentally observed a departure of measured values of Nusselt numbers from the theory, and the dependence of the departure upon the leading edge geometry as well as the wall temperature.

Attempts were made to explain the discrepancies emerging from comparisons of theory with experiment. Schmidt and Beckmann (1930) suggested that a plate length larger than the physical plate length be used for the calculation of the Grashof number to permit better agreement with data. The suggested method was used by Eichhorn (1962) to correct his experimental data for one location near the edge. Obviously, it is desirable to have sufficient experimental data for thermal boundary layers around the leading edge, including precise measurements of temperature profiles. Brodowicz (1968) experimentally investigated the thermal boundary layer existing around the leading edge of a vertical plate, and suggested an extension of the plate length to a virtual origin beyond the physical origin of the leading edge. Hieber (1974) analytically showed the breakdown of the boundary layer approximation in the vicinity of the leading edge by deriving a parametric form of the leading edge effect from a global heat-transfer rate. He also interpreted this leading indeterminancy as an apparent shift in the location of the leading edge.

In the present investigation, measurements were made for detailed temperature profiles around a 45-degree triangular type leading edge using a specklegram technique in order to define the range of the leading edge influence in terms of a critical Grashof number. The diagnostic aspects of the specklegram technique used are briefly described, and then the results of the thermal boundary layer growth and temperature profiles around the leading edge are discussed and compared with both theoretical and experimental data currently available.

2 Experiments

2.1 Vertical isothermal wall

The vertical isothermal wall, which was made of a 12.7 mm thick aluminum plate, is shown in Fig. 1. The dimensions of the heated plate were 254 mm by 254 mm. The plate was heated by a constant temperature bath. A plexi-glass water jacket with walls 9.5 mm in thickness was affixed to the back of the aluminum plate. Ethyleneglycol was circulated through 13 mm Tygon tubing. On the back side of the isothermal plate, nine thermocouples (Nickel-Aluminum/Chromium K type) were embedded 1 mm deep from the

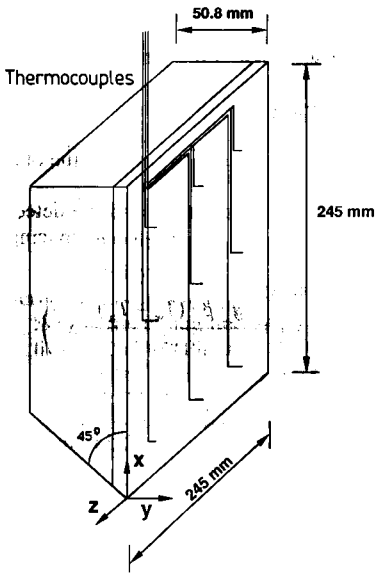

Fig. 1. A vertical isothermal wall with nine embedded thermocouples

front surface, so that the uniformity of the wall temperature could be monitored at all times. After the constant temperature bath reached steady state conditions, a temperature uniformity of less than 1% was attained for the nine spatially distributed thermocouples. The individual signal from each thermocouple was quite stable, and fluctuations in wall temperature were not detected.

2.2 Specklegram recording

Figure 2 presents the overall layout of the experimental setup with the specklegram system. A Spectra Physics 35 mW He-Ne laser of 632.8 nm wavelength was used as the coherent and monochromatic light source. The laser beam was collimated and then expanded to 120 mm in diameter using a microscope objective lens. The expanded beam was collimated again by a parabolic mirror 317.5 mm in diameter with a 1911.4 mm focal length to form parallel light rays throughout the test section. After passing through the test section, the light rays were turned and converged by the second parabolic mirror of focal length, $f=2552.7$ mm. The light rays after the focal point were illuminated on the ground glass which serves as the image plane of the test field, satisfying the relation $1/a+1/b=1/f$ where a and b represent the object distance from the test field to the second parabolic mirror and the image distance from the second parabolic mirror to the ground glass, respectively.

The average size of granules on the ground glass was 26 microns, which is equivalent to a 400 mesh screen. Speckles were formed spatially everywhere behind the ground glass because of the interference of randomly deflecting rays on the ground surface, as shown schematically in Fig. 3. Speckles were, therefore, formed regardless of the presence of a test field. The speckles formed by rays refracted by the presence of a nonuniform density or index-of-refraction field (test field) will have different spatial locations than speckles formed without any refraction. Each pair of speckles with and without refraction shares the same origination point on the ground glass, since the laser light was focused onto the ground glass. The amount of translocation of individual speckles has a precise relationship to the density or temperature where the rays are diffracted. A specklegram is made by taking a double-exposed photograph of those speckles on the focal plane without refraction and then with the speckles being translocated by refraction in the test field. The distances of the speckle translocations are measured using the principle of Young's fringes (Hecht, 1974).

The speckle formation is schematically illustrated in Fig. 4. Without going through a test field, the light rays diffracted by the ground glass, form a speckle, I, at the image plane of the specklegram. Because of density variations, the light rays refract at the test plane with a small angle, α, and form another speckle, I', at the image plane. From the geometrical similarity, assuming infinitesimally small angles of α and ε, the relationship is

$$\alpha = \varepsilon \cdot m \tag{1}$$

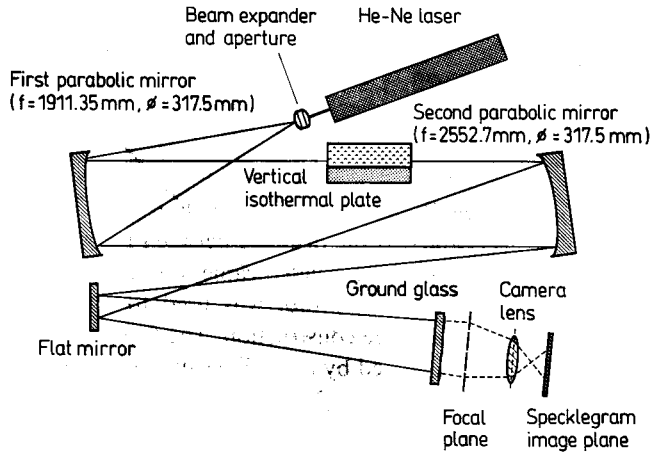

Fig. 2. A schematic diagram of the experimental setup

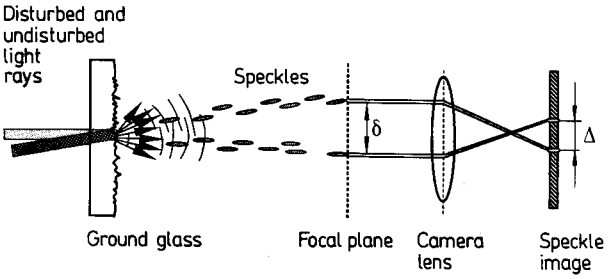

Fig. 3. A schematic illustration of speckle formation

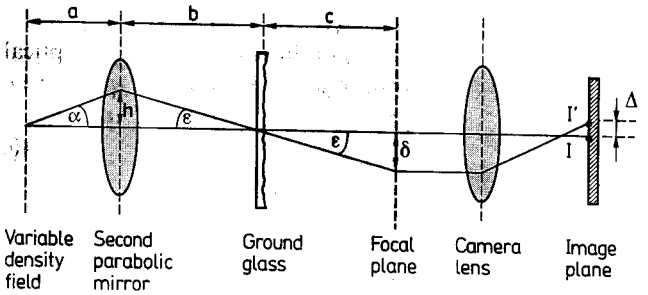

Fig. 4. An optical arrangement for speckle image construction

where the magnification, m, is defined as the ratio of the image distance to the object distance from the lens, i.e., $m=b/a$. The speckle dislocation is expressed as

$$\Delta = m' \cdot \delta \cong m' \cdot \varepsilon \cdot c \tag{2}$$

where m' represents the magnification of the camera lens, and c is the distance between the ground glass and the focal plane of the camera lens.

2.3 Speckle data interpretation

The evaluation of the fringe spacing was performed with a grey image processor, which digitally identifies points for the maximum and the minimum light intensity of a fringe pattern. The principle of Young's fringes states that the

fringe spacing, s, decreases with an increase of the translocated distance between an adjacent pair of speckles, Δ (Archbold et al., 1970), i.e.,

$$s = \frac{\lambda \cdot d}{\Delta} \tag{3}$$

where the wave length, λ, of the incident light is 632.8 nm for a He = Ne laser, and d is the distance between the specklegram and the screen, where a video camera was focused. A He = Ne laser with 5 mW power was used to illuminate specklegrams for the fringe construction. The fringe patterns were detected and digitized by the video camera and sent to the microprocessor for the evaluation of temperature. Combining Eqs. (2) and (3) gives an expression for the speckle dislocation at the focal plane:

$$\delta = \frac{\lambda \cdot d}{s \cdot m'}. \tag{4}$$

Considering Fermat's principle with a boundary layer simplification (Merzkirch, 1981), the diffraction angle of light rays in the y direction, α, can be expressed in terms of the index of refraction and a geometrical constant:

$$\alpha = \frac{\partial y}{\partial z} = \frac{1}{n} \cdot \frac{\partial n}{\partial y} \cdot L = \varepsilon \cdot m \tag{5a}$$

or with Eq. (2)

$$\alpha = m \cdot \varepsilon = \frac{\delta}{c} \cdot m = \frac{1}{n} \cdot \frac{\partial n}{\partial y} \cdot L \tag{5b}$$

where L indicates the length of the test section in the optical axis. The speckle disposition at the focal plane will also be

$$\frac{\partial n}{\partial y} = \frac{\delta \cdot m}{L \cdot c} \tag{6}$$

where the index of refraction of the media (air) is assumed to be close to unity for most cases (for example, n is 1.0002719 at 293 K, or 20 °C and one atmosphere pressure for air).

Using the Gladstone-Dale relationship (Vest, 1979) of

$$n = K \cdot \varrho + 1 \tag{7}$$

where the Gladstone-Dale constant K for air is taken as 0.2257×10^{-3} m^3/kg for $\lambda = 632.8$ nm (Merzkirch, 1987), Eq. (6) can be rewritten for the density variation as

$$\frac{\partial \varrho}{\partial y} = \frac{\lambda \cdot d}{L \cdot c \cdot s \cdot K} \cdot \frac{m}{m'}. \tag{8}$$

Equation (6) can also be expressed for the spatial temperature variation in terms of other known parameters and constants:

$$\frac{\partial T}{\partial y} = \frac{\lambda \cdot d}{L \cdot c \cdot s} \cdot \left(\frac{\partial n}{\partial T}\right)^{-1} \cdot \frac{m}{m'} \tag{9}$$

where the constant, $\partial n / \partial T$, is taken as 0.927×10^{-6} K^{-1} for air (Eckert and Goldstein, 1976) and all the other optical and geometrical parameters are specified so that the temperature gradient $\partial T / \partial y$ can be calculated with the measured fringe spacing, s. The temperature profiles were calculated by numerically integrating the temperature gradient with Simpson's rule (Carnahan et al., 1969).

The uncertainty associated with the fringe spacing measurements was estimated to be approximately ±15% by Sivasubramanian et al. (1984). In the present study, which employed a comprehensive digitizing of the fringes and a precise determination of the spacing by microcomputer, the fringe spacing measurement uncertainty was estimated to be within ±1%. The uncertainty associated with the other parameters in Eq. (9) should not exceed ±1%, since those parameters were determined from straightforward measurements or from well-established analyses. Therefore, the overall uncertainty for the present technique of temperature measurement is estimated to be on the order of 1 to 2%.

3 Results and discussion

Results are presented for: 1) the thermal boundary layer around the leading edge, 2) the temperature profiles around the leading edge as well as the downstream wall, and 3) the equivalent plate-length x_0 accounting for the edge influence on the temperature profile development. Measurements were made for four different x-locations and for five different wall temperatures ranging from 53.0 °C to 86.2 °C (326 K and 359.2 K, equivalently). A matrix of Grashof numbers for these experimental conditions is given in Table 1. The ambient temperature, T_∞, was maintained at 25 °C or 298 K for all tests.

In Fig. 5, photographs of the fringe patterns generated from a typical specklegram for $T_w - T_\infty = 61.2$ K are presented for five different locations inside and outside the thermal layer. Near the wall, where the temperature gradient is very steep, the fringes are very definite and the spacing are narrow (inset photo D). The fringe spacing becomes wider as the edge of the boundary layer is approached (inset photo E), and fringes disappear outside the thermal layer where there is no detectable dislocation of speckles (inset photo B). Around the leading edge, the orientation of fringes is altered since fringes (or the primary direction of speckle dislocation) must appear perpendicular to a local temperature gradient (inset photos A and C). Based on these distinctive character-

Table 1. Experimental Grashof numbers[a]

x (mm)	T_w (°C)				
	53.0	60.9	69.0	83.2	86.2
7.8	1,456.8	1,788.1	2,057.0	2,507.2	2,540.8
14.2	8,790.0	10,789.0	12,411.0	15,127.3	15,330.1
30.8	89,696.8	110,095.6	126,646.5	154,365.1	156,434.8
50.0	383,738.0	471,007.7	541,814.9	660,400.1	669,254.3

[a] Kinematic viscosity evaluated at the reference temperature $T_r = T_w - 0.38\,(T_w - T_\infty)$ suggested by Sparrow and Gregg (1958)

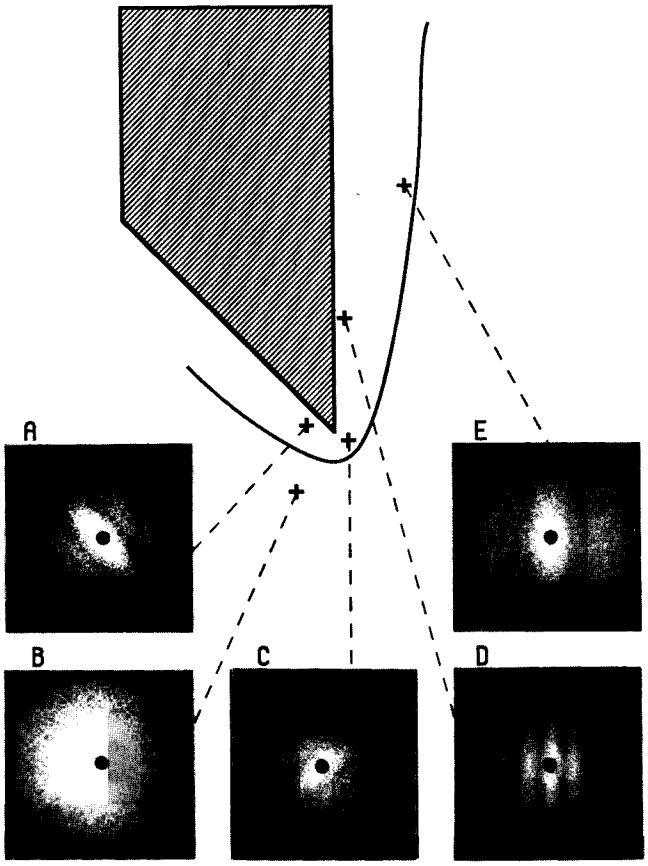

Fig. 5. Fringe spacing and orientation at five different locations around the leading edge for $T_w = 86.2$ °C

istics of fringe patterns in different locations, loci of the boundary of the thermal layer were determined, and results are presented as the black symbols in Fig. 6.

The solid curve in Fig. 6 represents a calculated thermal boundary profile (Eckert, 1950). The present specklegram data demonstrate an earlier and thicker layer development around the leading edge than is predicted by the theory, which assumes that the thermal layer begins abruptly at $x=0$. The thermal layer shown with the dashed curve was obtained by analyzing the interferogram result published by Sernas and Fletcher (1970), who employed a Wollaston prism interferometer technique. The analysis of the boundary identification was based on a criterion that the interferometric fringes, which should be parallel and equally spaced in the free stream, would alter their direction and spacing as the thermal boundary layer is approached. This criterion, however, can result in an erroneous estimation of the thermal boundary since the definite loci for the alteration of the fringe pattern are very difficult to determine.

Temperature measurements were made along the negative x-coordinate beyond the leading edge and are presented in Fig. 7 as a function of a dimensionless length x/H. The present data are compared with previously measured data by Brodowicz (1968), which are represented as the solid curve, and fairly good agreement is shown. The thickness of

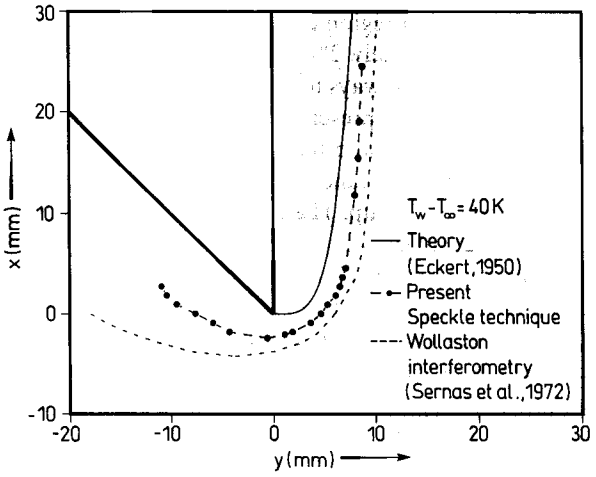

Fig. 6. Measured and calculated thermal boundary layers near the convection leading edge of a vertical isothermal wall

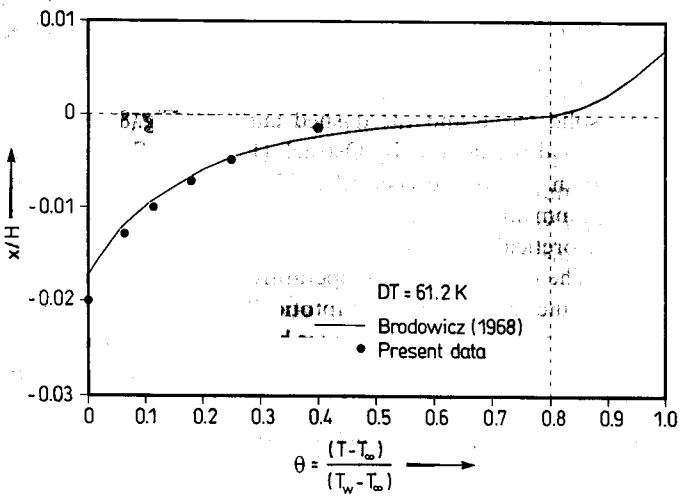

Fig. 7. Temperature profile measured in the pre-developed convection layer preceding the leading edge

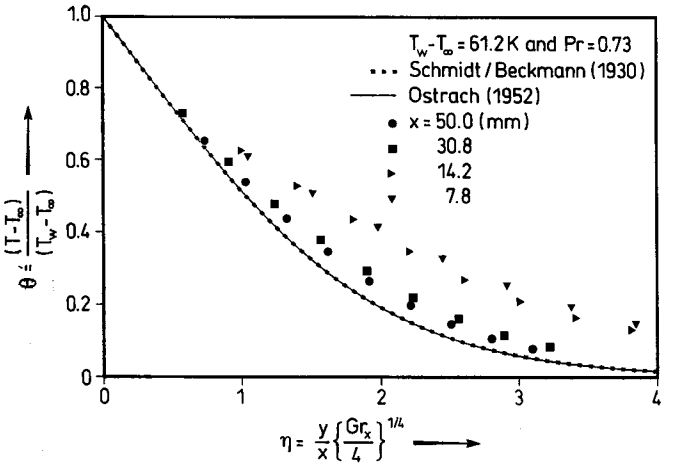

Fig. 8. Dimensionless temperature profiles as a function of dimensionless similarity variable at four different x locations for $T_w = 86.2$ °C

the thermal convection region extended to the negative x is shown to be approximately 2% of the plate length H.

There are two typical ways to present heat transfer correlation results. One is a presentation of Nusselt numbers versus Grashof numbers, and the other is to present dimensionless temperature as a function of Grashof number or a similar dimensionless group. The latter is more appropriate to present the current data for comprehensive inspection of individual temperature profiles. As the Nusselt numbers are calculated by integrating the heat convection coefficient $h(x, y)$, and the heat convection coefficient is evaluated from measured values of temperature, the discrepancy shown in temperature profiles can be diminished in the integration procedures for the case of Nusselt number presentation.

Figure 8 presents dimensionless temperature versus dimensionless variable, η, for the temperature difference of 61.2 K. Equation (9) was used to calculate the temperature profiles from the fringe spacing data. The reference temperature suggested by Sparrow and Gregg (1958) was used to evaluate the kinematic viscosity of air:

$$T_r = T_w - 0.38(T_w - T_\infty). \tag{10}$$

The solid curve and the dashed curve in Fig. 8 represent theoretical predictions by Ostrach (1952) and Schmidt and Beckman (1930), respectively. The temperature data at $x = 7.8$ mm and 14.2 mm show significant discrepancies from the theoretical predictions, which assumed an ideal leading edge. The dimensionless temperature function, θ, and similarity function, η, will asymptotically approach zero and infinity, respectively, as the outer boundary of thermal layer is approached. Near the leading edge, the thermal layer is thicker than an ideal one (Fig. 7) and thus, the measured temperature should be higher than the theoretical values for the same y or for the same η. This is clearly evident from the temperature profiles measured at $x = 7.8$ mm and 14.2 mm. The influence of the leading edge decreases with increasing x, and the theoretical prediction and the data show better agreement for $x = 30.8$ mm and 50.0 mm. Data for the other three wall temperature conditions showed virtually the same qualitative characteristics as seen in Fig. 8.

Data at $x = 14.2$ mm and $x = 50.0$ mm are presented for several different wall temperature conditions in Fig. 9. The empty symbols represent dimensionless temperature profiles measured at $x = 14.2$ mm where the edge influence is significant. Although the set of data obtained at $x = 14.2$ mm demonstrate a qualitative consistency within the data for four different wall temperature conditions, the data do not show very good agreement with the theoretical predictions. An attempted parametric correction of the data with the use of equivalent plate-length x_0 to redefine Grashof numbers was not successful since the discrepancies are scattered and independent of the specified wall temperatures. Since the leading edge effect dominates the development of temperature profiles in the vicinity of the leading edge, the theory, which is strictly based on a similarity assumption, does not describe the practical situation for the data attained at $x = 14.2$ mm.

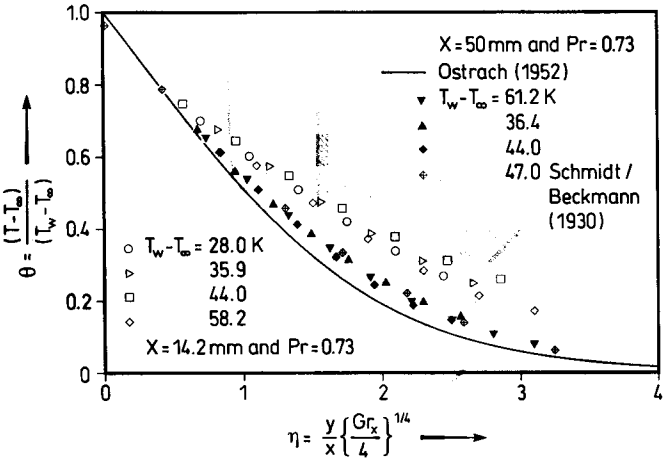

Fig. 9. Dimensionless temperature profiles as a function of dimensionless similarity variable measured at $x = 14.2$ mm and $x = 50.0$ mm for different wall temperatures

The solid symbols in Fig. 9 represent fairly well-developed temperature profiles away from the leading edge, at $x = 50.0$ mm, for three different wall temperatures. Also presented is a set of data obtained at the same x location by Schmidt and Beckmann (1930), who used a miniature thermocouple sensor to measure temperature. All the data sets for different wall temperatures show good agreement with the theoretical profile. The data exhibit slightly higher values than the predictions, which can be explained as a slight influence of the leading edge and will be discussed below.

Previous studies (Schmidt and Beckmann, 1930, Scherberg, 1962, Hieber, 1974) showed theoretically that the leading edge conditions for the case of an isothermal vertical wall, at a proper distance away from the edge, affected only the relative position of the boundary layers and not the similarity characteristics of velocity and temperature profiles. This has also been supported by a series of investigations by Yang and Jerger (1964), Suriano et al. (1965), and Suriano and Yang (1968), where the leading edge effect was analyzed based on a perturbation technique and a departure of their solutions from an ideal solution was shown when the Grashof number was less than 10^3. They also showed that the similarities of velocity and temperature profiles were eventually recovered when the Grashof number was high. Eichhorn (1962) demonstrated an improved comparison of the ideal solution with his limited experimental data employing the concept of an extended plate length.

In an attempt to attain a better comparison with theory, the dimensionless similarity function η was modified using an equivalent length scale, x_0, to replace x, the physical distance of the measurement location from the leading edge. The optimum value for x_0 was determined by adjusting x in the parameter η for the best fit of the data to the theoretical curve. For data taken at $x = 50.0$ mm, Fig. 10 shows the improved agreement with theory when the data are replotted using an x_0 of 68 mm for 61.2 K ($Gr_x = 6.69 \times 10^5$). Since the temperature profiles are fully developed at $x = 50$ mm,

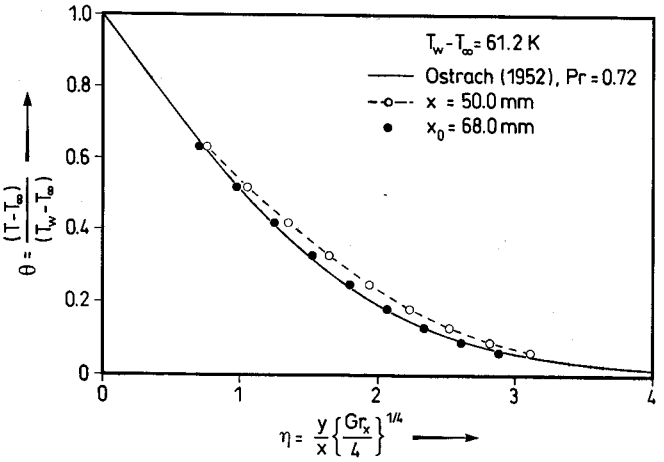

Fig. 10. Improved agreement with the theory for an equivalent wall length of $x_0 = 68$ mm for the data taken at $x = 50.0$ mm, for $T_w = 86.2$ °C

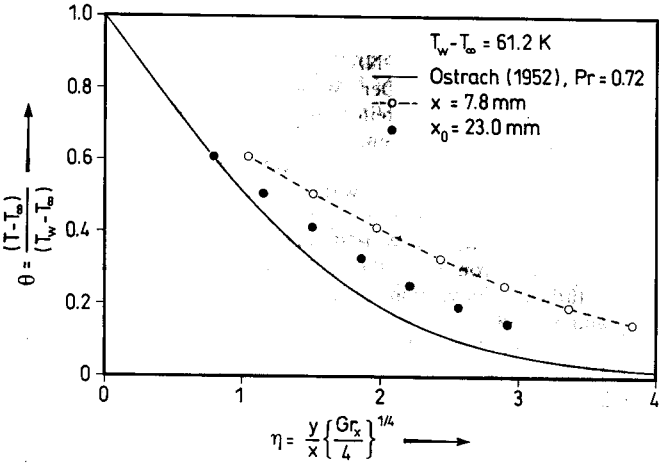

Fig. 11. Attempt of improved agreement with the theory for an equivalent wall length of $x_0 = 37$ mm for the data taken at $x = 14.2$ mm, for $T_w = 86.2$ °C

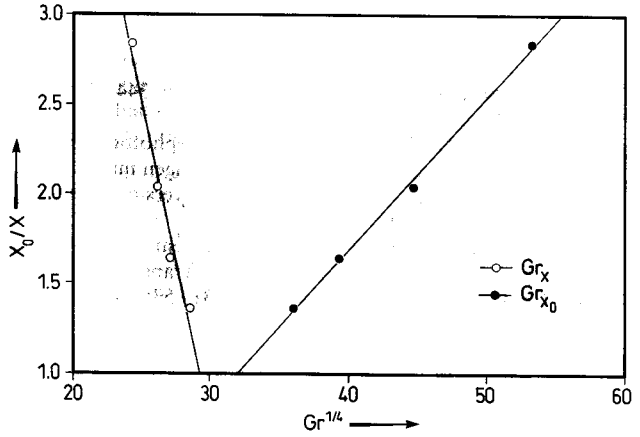

Fig. 12. The equivalence ratio x_0/x at $x = 50.0$ mm as function of the quadratic root of Grashof number based on x as well as x_0

the data plotted with an adjusted value of x, i.e., x_0, agree well with the theory, which is based on an assumption of the similarity principle.

Figure 11 represents the data measured at the x location of 7.8 mm ($Gr_x = 2.54 \times 10^3$) from the leading edge. The temperature difference was maintained the same (61.2 K) as in Fig. 10. The degree of comparison improvement for this case is not as distinctive as for the previous case of $x = 50$ mm. The measured temperature data, in fact, indicate strong non-similar behavior because the temperature profiles are not similarly developed near the edge. It was not feasible to determine an equivalent length that ensures improved agreement because of the lack of the similarity characteristics in the measured data. The theory, which assumes a similarity solution for the temperature profiles, fails to predict the temperature profiles at x locations closer than 50 mm from the leading edge for the current geometry.

Using the equations of motion and energy for the free-convection boundary layer, an analytical expression for the thermal boundary layer thickness may be easily derived (Holman, 1981) as

$$\frac{\delta}{x} = 3.93\, Pr^{-1/2} \cdot (0.952 + Pr)^{1/4} \cdot Gr_x^{-1/4}. \tag{11}$$

For a constant Prandtl number of 0.73 and constant thermodynamic properties (neglecting the dependence of kinematic viscosity on the wall temperature), Eq. (11) can be simplified to

$$\delta = \text{const} \cdot (T_w - T_\infty)^{-1/4} \cdot x^{1/4}. \tag{12}$$

As can be seen in Eq. (12), the effect of the isothermal wall is more prominent when the temperature is low, which results in a thicker boundary layer than that obtained at higher wall temperature under identical conditions. It is anticipated that for the case of a lower wall temperature the influence of the leading edge on the temperature profile is more prominent, and thus a longer equivalent length, x_0, is needed.

Figure 12 presents the extension ratio x/x_0 versus Grashof number defined in two different ways for four different wall temperatures. The empty symbols present the ratio x/x_0 in terms of Grashof number defined with the physical measurement location, $x = 50$ mm, and the solid symbols denote the same data plotted versus Grashof number based on the equivalent length, x_0. The two linearly interpolated lines intersect at about $Gr = 8.0 \times 10^5$ and the equivalent ratio of unity, as is expected since the values of Grashof numbers based on both length scales become identical at $x/x_0 = 1.0$.

It is anticipated that for Grashof numbers equal to or larger than 8.0×10^5, the theory predicts temperature profiles quite well without modifying the Grashof number. This was demonstrated in the work by Wernekinck (1985) where a similar measurement was made for Grashof number of 1.0×10^7. The leading edge influence diminished for the case of such a high Grashof number and the data showed very good agreement with the theory without being modified with a wall extension, i.e., $x_0 = x$.

4 Conclusions

The influence of a 45° leading edge on natural convection laminar boundary layer development along a vertical isothermal wall has been studied employing a He = Ne laser specklegram technique. By analyzing the characteristics of fringes, which are constructed from specklegrams based on Young's interference principle, detailed temperature profiles have been attained around the leading edge. The primary conclusions drawn from this study are:

1. Compared to other nonintrusive techniques such as interferometry, the speckle method is more convenient and reliable in investigating laminar natural convective thermal boundary layers.

2. In the vicinity of the lower end of a vertical isothermal wall, the leading edge effect is prominent, and the thermal boundary layer develops before the leading edge. As a consequence, the ideal theory that assumes an abrupt start of the thermal layer at $x=0$ does not properly describe the practical situation near the leading edge.

3. Since the leading edge influence decreases with increasing convective flow, the measured temperature profiles show fair agreement with the theory downstream away from the leading edge.

4. A linear decrease of x_0/x with $Gr_x^{1/4}$ (i.e., $x_0/x = -0.4 \cdot Gr_x^{1/4} + 12.63$) has been observed for Grashof numbers up to 8.0×10^5. For the range of $Gr_x \geq 8.0 \times 10^5$, the leading edge effect is minimal because of the dominant convective flows, and the theoretical prediction without the modification of an equivalent length, compares favorably with the present data.

Acknowledgements

The authors gratefully acknowledge Dr. Chris Burger at Texas A & M University for his help in setting up the digital imaging system for the fringe analysis. The research work has been possible with a financial support of the Engineering Excellence Grant Award for Young Faculty from Texas A & M University.

References

Archbold, E.; Burch, J. M.; Ennos, A. E. 1970: Recording of in-plane surface displacement by double-exposure speckle photography. Opt. Acta 17, 883–893

Brodowicz, K. 1968: An analysis of laminar free convection around isothermal vertical plate. Int. J. Heat Mass Transfer 11, 201–209

Carnahan, B.; Luther, H. A.; Wilkes, J. O. 1969: Applied numerical methods. pp. 71–75. New York: Wiley

Dainty, J. C. 1984: Laser speckle and related phenomena. Berlin Heidelberg New York: Springer

Eckert, E. R. G. 1950: Introduction to the transfer of heat and mass. pp. 158–171. New York: McGraw-Hill

Eckert, E. R. G.; Goldstein, R. J. (eds.) 1976: Measurements in heat transfer. p. 241. New York: McGraw-Hill

Eckert, E. R. G.; Soehngen, E. E. 1948: Studies on heat transfer in laminar free convection with the Zehnder-Mach interferometer. USAF Tech. Report 5747, Dayton/OH: Air Material Command

Eichhorn, R. 1962: Measurement of low speed gas flows by particle trajectories: a new determination of free convection velocity profiles. Int. J. Heat Mass Transfer 5, 915–928

Erbeck, R. 1985: Fast image processing with a microcomputer applied to speckle photography. Appl. Opt. 24, 3838–3841

Gryzagoridis, J. 1973: Leading edge effects on Nusselt number for a vertical plate in natural convection. Int. J. Heat Mass Transfer 16, 517–520

Gryzagoridis, J. 1978: Leading edge geometry effects on natural convection from an isothermal vertical plate. Letters in Heat Mass Transfer 5, 203–213

Hecht, E. 1974: Optics. pp. 339–346. New York: Addison-Wesley

Hieber, C. A. 1974: Natural convection around a semi-infinite vertical plate: higher-order effects. Int. J. Heat Mass Transfer 17, 785–791

Holman, J. P. 1981: Heat Transfer (5th ed.). pp. 266–272. New York: McGraw-Hill

Merzkirch, W. 1981: Density sensitive flow visualization. In: Methods of experimental physics (ed. Emrich, R. J.). Vol. 18, Part A, 345–403, New York: Academic Press

Merzkirch, W. 1987: Flow visualization (2nd ed.). pp. 118–122. New York: Academic Press

Ostrach, S. 1952: An analysis of laminar free-convection flow and heat transfer about a flat plate parallel to the direction of the generating body force. NACA Rep. TN-2635

Pohlhausen, E. 1921: Der Wärmeaustausch zwischen festen Körpern und Flüssigkeiten mit kleiner Reibung und kleiner Wärmeleitung. Z. Angew. Math. Mech. 1, 115–121

Scherberg, M. G. 1962: Natural convection near and above thermal leading edges on vertical walls. Int. J. Heat Mass Transfer 11, 1001–1010

Schmidt, E.; Beckmann, W. 1930: Das Temperatur- und Geschwindigkeitsfeld von einer Wärme abgebenden senkrechten Platte bei natürlicher Konvektion. Tech. Mech. Thermodynam. 1, 341–349 and 391–406

Sernas, V.; Fletcher, L. S. 1970: A schlieren interferometer method for heat transfer studies. J. Heat Transfer 92, 202–204

Sernas, V.; Fletcher, L. S.; Jones, J. A. 1972: An interferometric heat flux measuring device. Trans. Inst. Soc. Am. 11, 346–357

Sivasubramanian, M. S.; Cole, R.; Sukanek, P. C. 1984: Optical temperature gradient measurements using speckle photography. Int. J. Heat Mass Transfer 27, 773–780

Sparrow, E. M.; Gregg, J. L. 1958: The variable fluid problem in free convection. J. Heat Transfer 78, 1823–1828

Suriano, F. J.; Yang, K. T. 1968: Laminar free convection about vertical and horizontal plates at small moderate Grashof numbers. Int. J. Heat Mass Transfer 11, 473

Suriano, F.; Yang, K. T.; Donlon, J. A. 1965: Laminar free convection along a vertical plate at extremely small Grashof numbers. Int. J. Heat Mass Transfer 8, 815–831

Vest, C. M. 1979: Holographic interferometry. pp. 344–345. New York: Wiley

Wernekinck, U. 1985: Anwendung der Specklephotographie zur Sichtbarmachung und Messung von Strömungen mit veränderlicher Dichte. Ph.D. Thesis, Bochum University, Germany. Reihe 8-95. Berlin: VDI Verlag

Wernekinck, U.; Merzkirch, W. 1986: Measurement of natural convection by speckle photography. In: Heat Transfer (eds. Tien, C. L.; Carey, V. P.; Ferrell, J. K.). pp. 531–535. Washington: Hemisphere

Yang, K. T.; Jerger, E. W. 1964: First-order perturbations of laminar free-convection boundary layers on a vertical plate. J. Heat Transfer 8, 107–115

Received November 19, 1991